Int. J. Heat Mass Transfer. Vol. 27, No. 8, pp. 1365–1378, 1984
Printed in Great Britain

0017–9310/84 $3.00 + 0.00

FILM BOILING ON A REACTIVE SURFACE

MICHAEL EPSTEIN, JOSEPH C. LEUNG, GEORGE M. HAUSER and ROBERT E. HENRY
Fauske & Associates, Inc., 16W070 West 83rd Street, Burr Ridge, IL 60521, U.S.A.

and

LOUIS BAKER, JR.
Argonne National Laboratory, 9700 South Cass Avenue, Argonne, IL 60439, U.S.A.

(*Received* 6 *May* 1983 *and in revised form* 21 *November* 1983)

Abstract—To help understand the rapid oxidation of high-temperature materials immersed in water, we treat here the flow of a liquid over a reactive body; the temperature of the body is such that the liquid undergoes film boiling at its surface. Contained within the film that envelopes the surface is the evaporated liquid which diffuses to the surface and reacts there to form product gas which diffuses away from the surface. The two-phase flow and heat and mass transfer problem which arises is formulated within the framework of steady-state stagnation flow theory. The theory is applied to the quasi-steady oxidation of molten zirconium spheres falling through water and predicts results which are consistent with available zirconium sphere oxidation data.

NOMENCLATURE

- a stagnation point velocity gradient for the product gas–vapor film, equation (17)
- a_1 stagnation point velocity gradient for the liquid, equation (14)
- A dimensionless wall superheat parameter, equation (31)
- B dimensionless liquid subcooling parameter, equation (31)
- c heat capacity
- C pre-exponential factor in chemical rate equation (36)
- D Fick's molecular diffusion coefficient for the product gas–reactant vapor pair (H_2–H_2O)
- e total emittance of the reactive surface, equation (4)
- ΔE activation energy in chemical rate equation (36)
- f dimensionless product gas–vapor film flow stream function, equation (16)
- F dimensionless liquid flow stream function, equation (15)
- F_m fraction of unreacted molten metal sphere
- ΔH heat release per mole of metal reacted, equation (38)
- k thermal conductivity
- L latent heat of liquid evaporation
- L_m latent heat of fusion of metal sphere material
- $\dot{m}_v, \dot{m}_g$ vapor and product gas mass flux, respectively [kg m^{-2} s^{-1}]
- $\dot{m}$ total mass flux in product gas–vapor film, $\dot{m}_g + \dot{m}_v$
- M molecular weight or metal species
- n moles of reactant vapor (H_2O) removed per mole of metal reacted, equation (1)
- p pressure in the product gas–vapor film
- p_{eq} saturation pressure of the vapor at the vapor–liquid interface, equation (7)
- P pressure in the liquid, equation (13)
- P_0 reference pressure, equation (13)
- Pr Prandtl number, ν/α
- $\dot{q}$ convective heat flux at the reacting surface, equation (39)
- $\dot{q}_{rad}$ radiation hat flux at the reacting surface, equation (4)
- Q_{rad} dimensionless radiation heat flux, equation (30)
- r radial (or arc length) measured from the stagnation point, Fig. 1.
- R radius of reacting sphere
- $\bar{R}$ universal gas constant, equation (36)
- Re Reynolds number of falling sphere, $2RV_\infty/\nu_l$
- Sc Schmidt number, ν/D
- t, T product gas–vapor film and liquid temperatures, respectively
- T_m temperature of reacting metal sphere
- T_w temperature of reactive surface, Fig. 1
- u, U product gas–vapor film and liquid velocities in the r-direction, respectively, Fig. 1
- v, V product gas–vapor film and liquid velocities in the z-direction, respectively, Fig. 1
- x radial location of reaction (oxidation) front in reacting metal sphere
- Y mass fraction of reactant vapor
- z coordinate normal to the reacting surface, Fig. 1.

Greek symbols

- α thermal diffusivity
- β $(\nu\rho^{1/2})^{1/2}$ ratio, equation (30)
- δ product gas–vapor film thickness, Fig. 1
- ε density ratio, equation (30)
- η dimensionless similarity coordinate for product gas–vapor film, equation (16)

η_δ	dimensionless vapor film thickness, $\delta(2a/v)^{1/2}$
θ	dimensionless product gas–vapor film temperature, equation (18)
μ	absolute viscosity
ν	kinematic viscosity
ξ	dimensionless similarity coordinate for the liquid, equation (15)
ρ	density
σ	Stefan–Boltzmann radiation constant, equation (4)
τ	time
ϕ	dimensionless liquid temperature, equation (18)
ω	dimensionless mass fraction of reactant vapor, equations (18) or (33).

Subscripts*

g	product gas (H_2)
i	at boiling vapor–liquid interface, Fig. 1
l	liquid properties
m	reacting metal sphere
v	reactant vapor (H_2O)
w	at the reactive surface (wall), Fig. 1
∞	conditions in the liquid far from the reactive surface.

INTRODUCTION

THERE are many chemical reacting flow processes in which, under certain circumstances, the reaction takes place only at solid or liquid surfaces. Prediction of the extent of reaction is frequently complicated by the intervention of fluid phase diffusional limitation (on reactant supply and product escape) which introduce a dependence of the reaction rate on fluid dynamic and transport properties. Previous studies of convective diffusion to a reactive surface have been concerned, for the most part, with surfaces immersed in mainstream flows of either pure liquid or gas. In the case of heterogeneous reactions in which the surface material is a bona fide reactant (as opposed to a catalyst) there will be a net interfacial velocity that may produce significant effects on the convective transfer coefficient. This fact has motivated much of the past theoretical work on boundary layer flows of single-phase fluids with 'blowing' or 'suction' at the wall [1]. There is a need for comparable boundary layer analyses in which the reactive surface is submerged within a liquid reactant undergoing film boiling at the surface. The combined effects of two-phase flow and heterogeneous reactions (surface suction or blowing) are of interest, for example, in predicting the oxidation rates of molten metals in contact with water. This oxidation process is of importance in the assessment of hypothetical severe core damage accidents for light water reactors.

A number of experimental studies of the reaction of molten zirconium (Zr) metal quenched in water have been reported [2–6]. Among these, only the experiments of Crooks *et al.* [5] and Baker and Just [6] were carried out under controlled conditions. In the former study, a series of drop tests were performed in which the bottom end of vertically oriented Zr rods were melted inductively in an argon environment and allowed to drop into water. The droplets produced by this melting technique oxidized while falling freely through the water. The time and distances of fall through the water of the nominal 5.1 mm drops indicated a velocity of fall of approximately 90 cm s^{-1}. The thickness of the oxide layer beneath the surface of the reacted droplet was measured. In the experiments of Baker and Just [6], 2.54 cm lengths of either 30 or 60 mil diameter Zr wires were rapidly heated under water by a condenser discharge method. As the wire temperature increased and exceeded the melting temperature, the molten metal changed from an intact wire to a collection of droplets. The average droplet size decreased with increasing energy delivered to the wire and fell within the range of 0.1–2 mm. Evaluation of the extent of oxidation showed that more reaction occurs in heated water than in water at room temperature. In addition, the reaction was observed to depend strongly on the effective droplet sizes generated by the rapid heating.

Lustman [7] was the first to develop a model for predicting the extent of oxidation of molten Zr droplets falling through water. The droplet was assumed to be spherical with uniform temperature and cooled by radiation only. He used the low temperature data of Bostrom [8] for the isothermal oxidation of solid Zr in water for estimating the reaction kinetics of the problem. Hogan *et al.* [9] tried to improve upon Lustman's model by recognizing that the water surrounding the molten metal sphere must be in film boiling and, therefore, that the sphere loses energy by two heat transfer mechanisms: radiation and forced-convection film boiling. They used the correlation of Bromley *et al.* [10] for film boiling heat transfer from cylinders and concluded that the two modes of heat transfer are of equal importance. As in Lustman's model, the chemical heating of the sphere was assumed to depend on a surface reaction rate extrapolated from Bostrom's data. Numerical studies which included the effects of heat conduction (nonuniform temperatures) within the sphere and the systematic variation of physical parameters did not bring the predicted values of the extent of reaction in line with the observations of Crooks *et al.* [5].

Baker and Just [6], to account for the results of their Zr dropet–water reaction experiments, postulated that the heterogeneous reaction is fast enough, at least early in the quenching process, to cause the instantaneous oxidation rate to be limited by the rate at which water vapor can diffuse across the steam–hydrogen film that must surround the Zr sphere. In their quasi-steady-state model of a molten metal sphere quenching in water, the diffusion of steam toward the molten metal

* Unsubscripted physical properties α, μ, ρ, k, ν, and D pertain to the product gas–vapor film.

surface was formulated as a mass transfer coefficient for a motionless sphere times the vapor pressure of water evaluated at the bulk water temperature. Based on the two previous experimental studies [5, 8] and model predictions, a parabolic 'heterogeneous' reaction rate law (internally solid-state diffusion controlled) was chosen by Baker and Just [6] for comparison with the predicted external H_2O–H_2 diffusion-limited reaction rate. Indeed, the gaseous diffusion process within the H_2O–H_2 film limited the reaction rate initially until the buildup of an oxide film beneath the surface of the metal sphere reduced the parabolic rate to a lower value. The parabolic reaction law was assumed to control the reaction thereafter, leading to a predicted stage of net sphere cooling. The computed results for the final extent of reaction in heated water were generally in agreement with the experimental values. However, to obtain agreement with the results for the room temperature water experiments, it was necessary to arbitrarily increase the water vapor pressure at the steam vapor interface, which drives the gaseous diffusion process. This difficulty with the Baker–Just Zr-sphere-quenching model can be traced to the fact that the steam pressure at the steam–water interface is not determined solely by the temperature of the water, but depends on a balance between the processes of liquid convection and steam diffusion as well.

An objective of this paper is to present for the first time a boundary layer treatment of film boiling of a flowing liquid over a hot, *reactive* surface with due consideration of the effects of liquid subcooling, forced convection, counter-diffusion of product gas away from the surface and reactant vapor toward the surface, and nonzero net mass transfer at the reacting surface and at the boiling liquid surface. In particular, we formulate a steady-state theory of forced convection film boiling from a surface undergoing heterogeneous reaction with the evaporated liquid based on the mass, momentum and energy conservation principles for axisymmetric stagnation flow. This flow configuration approximates that in the experimental studies of hot metal spheres falling through water. In fact, the stagnation flow model has already proved to be quite useful in correlating heat transfer data for forced convection film boiling from inert spheres or cylinders [11]. The predictions of the model are subjected to a comparison with the Zr sphere oxidation measurements of Crooks *et al.* [5] and Baker and Just [6]. The agreement between theory and the experimental trends for Zr oxidation in both room temperature and heated water is quite satisfactory, and thus lends support to the analytical model.

ANALYSIS

Physical model and coordinate system for steady-state oxidation

Figure 1 shows a sketch of the physical model and coordinate system used for the present study. We consider a hot, reactive surface (C, W, Fe, U, Zr, UO_2, etc.) placed normal to a stream of liquid reactant (water)

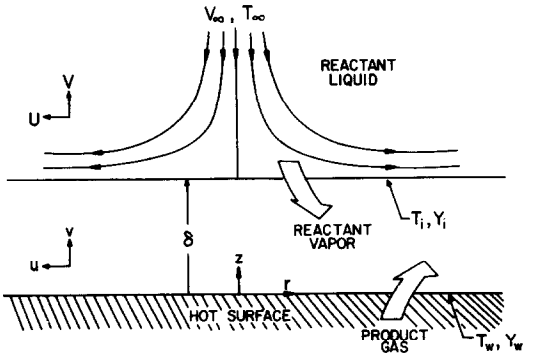

FIG. 1. Schematic of stagnation flow model.

which has a uniform constant velocity, V_∞ at infinity. The surface is assumed to act as a stationary solid surface, even when in the molten state (owing to, say, the formation of oxide scale). The surface temperature, T_w, is assumed constant and sufficiently high so that the surface is separated from the liquid by a continuous film of reactant vapor (and gas product; see below). The temperature of the liquid at infinity is T_∞ which, as we shall see, may be lower or *higher* than the temperature at the vapor–liquid interface, T_i.

A steady-state counter flux transport process is brought about in the film by the reaction of the evaporated liquid and the reactive surface. For example, when water flows over a hot metal surface M, the water vapor and metal react forming inert hydrogen gas in accord with the stoichiometry

$$\mathrm{M(s\ or\ l)} + n\mathrm{H_2O(v)} \rightarrow \mathrm{MO}_n\mathrm{(s)} + n\mathrm{H_2(g)}, \qquad (1)$$

where v, g, s, and l indicate vapor, gas, solid and liquid, respectively. The formation of metal oxide MO_n provides a sink for the water vapor and the production of H_2, resulting in the counter flux of these two species. Since the surface reaction acts as a mass sink for the heavier vapor species (H_2O), strong convective inflows of vapor may be induced, leading to concentration and temperature profiles in the steam–hydrogen film which are not linear. The product H_2 gas does not pass through the vapor–liquid interface, thus, in order to achieve steady-state conditions, the H_2 gas must be expelled in the radial direction, r, by the liquid shear acting on the steam–H_2 film.

It is important to note that whenever there are concentration and temperature gradients in a gas mixture, the processes of thermal diffusion and diffusional conduction come into play. The first of these is a transport of mass owing to a temperature gradient, while the second is an energy transport owing to a concentration gradient. Their effects are not insignificant in gas mixtures with both large molecular weight disparities and large temperature gradients. An example is the H_2–H_2O product gas–vapor film mixture produced during a metal–water reaction and of interest here. Moreover, effects which inevitably accompany thermal diffusion are those due to variable gas mixture properties. The present work may be regarded as a first step in the boundary layer treatment

of metal–water reactions in that variable mixture properties and the processes of thermal diffusion and diffusional conduction are not accounted for. The fact that in the physical situation studied here there are two boundary layers (gas–vapor film and liquid) and two interfaces across which energy and mass are transported (reacting surface and vapor–liquid interface) already makes for numerical difficulties well beyond those encountered in typical boundary layer problems. The task of obtaining solutions that also includes thermal diffusion, diffusional conduction and variable properties would indeed be a formidable numerical undertaking. Estimates based on the solutions obtained herein for the water–Zr system indicate that the effects of thermal diffusion and diffusional conduction are to modify local mass and energy fluxes within the product gas–vapor film by at most about 20 and 50%, respectively. As far as general trends are concerned, experience with other combined heat and mass transfer problems has shown that the complete consideration of mixture property variations and diffusional effects does not alter the findings of the constant property, 'ordinary' concentration (Fick) diffusion analysis in an essential way. What with the uncertainty factors such as instabilities and wave motion which occur in film boiling, geometry changes during reaction, and the sudden evolution of product gas which propels and spins the reacting particle, there may be little justification to strive for the more 'accurate' treatment that incorporates property variations and all modes of diffusional transport.

The thickness of the vapor–product gas film is assumed to be spatially uniform. From stagnation flow theory, it is known that both the boundary layer thickness and the rate of heat transfer from the liquid in the z-direction are independent of the radial distance, r. Thus, we anticipate that the gas–vapor film has a uniform thickness. The thickness of the gas–vapor film, δ, and the temperature, T_i, and the vapor mass fraction, Y_i, at the liquid surface, as well as the vapor mass fraction, Y_w, at the reactive surface are unknown and must be determined from the solution.

In the presentation that follows, it is convenient to subdivide the analysis into two portions: one dealing with a steady-state system in which the reaction rate is limited by the rate at which the reactant can diffuse across the product gas–vapor film by Fick diffusion, and the second dealing with the quasi-steady oxidation of a hot reactive sphere in water when the rate of reaction is not completely diffusion controlled and given by a specific phenomenological chemical kinetic rate law. The former situation will allow us to readily illustrate some interesting aspects of film boiling with diffusion in the film, while the latter will enable us to compare the stagnation flow theory with experiment.

The equations and the boundary conditions for diffusion control in the gas–vapor film

The underlying conservation equations that apply to the model described in the foregoing are those for laminar, steady axisymmetric stagnation flow. As mentioned in the foregoing, we will assume that constant average values can be assigned to the physical properties of the fluids. The vapor is assumed to react instantaneously at the reactive surface so that the mass fraction of vapor at this location $Y_w = 0$. Across the vapor–liquid interface at $z = \delta$, velocity, shear stress, vapor, and gas mass flow continuity requirements provide the matching conditions

$$u = U, \quad \mu\frac{\partial u}{\partial z} = \mu_l\frac{\partial U}{\partial z}, \quad \rho v = \rho_l V, \quad \dot{m}_g = 0. \tag{2}$$

In addition, temperature and energy continuity is also required at this interface

$$t = T = T_i, \quad k\frac{\partial t}{\partial z} = \rho v L + k_l\frac{\partial T}{\partial z} + \dot{q}_{rad}. \tag{3}$$

Upper case letters are used to identify the liquid velocity and temperature variables, while those in the vapor film are assigned lower case letters. Unsubscripted physical properties, μ, ρ, and k, pertain to the product gas–vapor film, while those in the liquid region bear the subscript l. The term $\dot{q}_{rad}$ in equation (3) represents the radiation heat flux from the hot solid surface to the liquid surface and is estimated with the Stefan–Boltzmann law

$$\dot{q}_{rad} = e\sigma T_w^4. \tag{4}$$

Clearly, back radiation from the relatively cold liquid surface has been neglected, and it is assumed that thermal radiation is neither absorbed nor emitted in the gas–vapor film. The condition on the gas mass flux in equation (2) follows from the fact that the liquid surface is assumed to be impermeable to the product gas species. Another condition on the 'evaporation' velocity v normal to the liquid surface at $z = \delta$ is obtained from Fick's law of binary diffusion

$$\dot{m}_v - Y(\dot{m}_v + \dot{m}_g) = -\rho D\left(\frac{\partial Y}{\partial z}\right). \tag{5}$$

By setting $\dot{m}_g = 0$ and $\dot{m}_v = \rho v$, we get

$$v(\delta) = -\frac{D}{1 - Y_i}\left(\frac{\partial Y}{\partial z}\right)_{z=\delta}. \tag{6}$$

Finally, the concentration of the reactant vapor at the liquid surface Y_i and the corresponding partial pressure of the vapor are related by the definition

$$\frac{p_{eq}(T_i)}{P_\infty} = \left[1 + \frac{M_v}{M_g}\left(\frac{1}{Y_i} - 1\right)\right]^{-1}. \tag{7}$$

The above expression, in fact, relates the liquid surface temperature T_i to Y_i since the interface at $z = \delta$ is a saturation state for the vapor.

The boundary conditions imposed at the hot reacting surface are

$$z = 0; \quad u = 0, \quad t = T_w, \quad Y = Y_w = 0. \tag{8}$$

The last equation follows directly from our assumption that mass transfer through the film controls the reaction rate at $z = 0$. This assumption will be relaxed

in a later section. To determine the boundary condition on the normal velocity v at the reacting surface, we write from the stoichiometry of the surface reaction in water [see e.g. equation (1)]

$$\frac{\dot{m}_g}{M_g} = -\frac{\dot{m}_v}{M_v}. \tag{9}$$

From equation (5) evaluated at $z = 0$ and equation (9), the total mass flux at $z = 0$ is

$$\dot{m}(0) = \dot{m}_g + \dot{m}_v = -(1 - M_g/M_v)\rho D\left(\frac{\partial Y}{\partial z}\right)_{z=0}, \tag{10}$$

or, since $\dot{m}(0) = \rho v(0)$

$$v(0) = -(1 - M_g/M_v)D\left(\frac{\partial Y}{\partial z}\right)_{z=0}. \tag{11}$$

In this equation, $v(0)$ represents the interfacial velocity at $z = 0$ due to chemical reaction. Depending on whether M_g/M_v is greater than or less than unity, $v(0)$ represents a blowing or suction effect, respectively. The net mass flux will be toward the reacting surface (suction) in the hydrogen–steam film since $M_g/M_v = 1/9$ for this system.

The boundary conditions in the liquid flow at infinity are

$$y \to \infty; \quad U \to a_1 r, \quad V \to V_\infty = -2a_1 z, \quad T \to T_\infty, \tag{12}$$

$$P \to P_\infty = P_0 - \tfrac{1}{2}a_1^2 \rho_l (r^2 + 4z^2). \tag{13}$$

Equations (12) and (13) simply express the fact that the liquid flow field and pressure distribution away from the liquid-film interface is that for potential flow. The constant a_1 in these equations is the stagnation point velocity gradient. The analysis presented here may be regarded as applicable to the chemical reaction and flow conditions in the neighborhood of the forward stagnation point of a metal sphere by simply setting

$$a_1 = \frac{3V_\infty}{2R}, \tag{14}$$

where R is the radius of the sphere.

Similarity transformation

To bring the problem into a more tractable form, we introduce a change of variables by means of the usual boundary layer similarity transformation for axially symmetric stagnation flow. In particular, for the liquid momentum field, we define the variables

$$\xi = (2a_1/\nu_l)^{1/2} z, \quad U = a_1 r F'(\xi), \quad V = -(2a_1\nu_l)^{1/2} F(\xi). \tag{15}$$

Similarly, for the vapor–gas film there is introduced

$$\eta = (2a/\nu)^{1/2} z, \quad u = arf'(\eta), \quad v = -(2a\nu)^{1/2} f(\eta), \tag{16}$$

where a is the stagnation point velocity gradient for the vapor–gas film and is related to a_1 according to

$$a = (\rho_l/\rho)^{1/2} a_1. \tag{17}$$

This follows from the fact that the radial variation of pressure within the liquid flow ($\partial P/\partial r = -a_1^2 \rho_l r$) and within the film flow ($\partial p/\partial r = -a^2 \rho r$) must be the same—a consequence of the nature of boundary layers. The primes in equations (15) and (16) denote differentiation with respect to the independent variables ξ and η, respectively. Finally, the temperature profiles and the vapor mass fraction profile are conveniently described in terms of the following dimensionless choice:

$$\phi = \frac{T(\xi) - T_i}{T_\infty - T_i}, \quad \theta = \frac{t(\eta) - T_w}{T_i - T_w}, \quad \omega = \frac{Y(\eta)}{Y_i}. \tag{18}$$

When the transformations defined by equations (15), (16), and (18) are introduced into the governing partial differential equations of momentum, heat, and mass transfer for axisymmetric stagnation flow, there results the well-known forms

$$F''' + F'' + \tfrac{1}{2}(1 - F'^2) = 0, \tag{19}$$

$$\phi'' + Pr_l F\phi' = 0, \tag{20}$$

for the liquid region and

$$f''' + ff'' + \tfrac{1}{2}(1 - f'^2) = 0, \tag{21}$$

$$\theta'' + Pr\, f\theta' = 0, \tag{22}$$

$$\omega'' + Sc\, f\omega' = 0, \tag{23}$$

for the gas–vapor film, where $Pr = \nu/\alpha$ is the Prandtl number and $Sc = \nu/D$ is the Schmidt number.

The boundary and matching conditions may also be rephrased in terms of the similarity variables. First, it may be noted that, at the liquid surface, $z = \delta$, and correspondingly the value of η at the interface is denoted by $\eta_\delta = (2a/\nu)^{1/2}\delta$. The value of ξ at the liquid surface might also be denoted by ξ_δ. However, since the actual value of ξ does not enter in the differential equations nor in the boundary conditions, we can, without any loss of generality, take $\xi = 0$ at the liquid surface. Then applying the transformations defined in equations (15), (16), and (18) to the matching and boundary conditions, equations (2), (3), (6), (8), and (11)–(13), there is obtained

$$\eta = 0: \quad f(0) = \frac{Y_i \omega'(0)}{Sc}\left(1 - \frac{M_g}{M_v}\right),$$

$$f'(0) = \theta(0) = \omega(0) = 0, \tag{24}$$

$$\eta = \eta_\delta: \begin{cases} F(0) = \varepsilon\beta f(\eta_\delta), \quad F'(0) = \dfrac{1}{\varepsilon} f'(\eta_\delta), \\ \qquad\qquad F''(0) = \beta f''(\eta_\delta), & (25) \\ \phi(0) = 0, \quad \theta(\eta_\delta) = 1.0, \quad \omega(\eta_\delta) = 1.0, & (26) \\ Y_i = \left[1 + \dfrac{\omega'(\eta_\delta)}{Sc\, f(\eta_\delta)}\right]^{-1}, & (27) \\ A\theta'(\eta_\delta) + Q_{rad} = f(\eta_\delta) + B\phi'(0), & (28) \end{cases}$$

$$\xi \to \infty: \quad F'(\xi) \to 1.0, \quad \phi(\xi) \to 1.0. \tag{29}$$

In the matching conditions, equations (25) and (28), ε, β,

A, B, and Q_{rad} are dimensionless parameters defined as

$$\varepsilon = \left(\frac{\rho}{\rho_l}\right)^{1/2}, \quad \beta = \left[\left(\frac{\rho}{\rho_l}\right)^{1/2}\frac{\nu}{\nu_l}\right]^{1/2},$$

$$Q_{rad} = \frac{\dot{q}_{rad}}{(2a/\nu)^{1/2}Lv\rho}, \quad (30)$$

$$A = \frac{c(T_w - T_i)}{Pr\,L}, \quad B = \beta\frac{k_l}{k}\frac{c(T_i - T_\infty)}{Pr\,L}. \quad (31)$$

The last two of these parameters are somewhat special inasmuch as the liquid surface temperature T_i is one of the unknowns of the problem; therefore, they cannot be treated as parameters whose values may be prescribed.

Solution method

In appraising any plan for numerical evaluation of the foregoing equations, cognizance must be taken of the large number of parameters involved. Even a minimal numerical study involving two values of each of the nine independent parameters would require consideration of 512 separate cases. Although, in principle, there is no limitation on the values of the parameters selected for the numerical solutions, there is a practical limit on the amount of numerical work which is feasible to present. Thus, values of the parameters appropriate to the Zr metal–water system were selected. This is in recognition of the fact that the oxidation of molten Zr submerged in water is of great practical interest and is additionally the system for which experiments have been performed. Since we are dealing with a metal–water system, $M_v = 18.02$ for the reactant water vapor species and $M_g = 2.016$ for the gas product species H_2. Estimates of the physical properties of hydrogen–steam mixtures indicated that the Prandtl number is fairly insensitive to both composition and temperature and is well represented by $Pr = 0.7$. The Schmidt number, however, varies greatly with composition; it was assumed that $Sc = 0.4$, a value typical of H_2O–H_2 mixtures with low mass fractional concentrations of H_2. This choice of a constant Sc is one of the weaker points of the theory, but any attempt at accounting for the variation of Sc with composition would be very tedious. Values of the liquid Prandtl number $Pr_l = 2.0$, 7.0 and the viscosity ratio $\beta = 3.0$, 5.0 were assigned to approximately cover the temperature range in the water under room temperature and heated conditions, respectively. The bulk of the solutions were carried out for $\varepsilon = 0.005$, but some results were obtained at different values of ε and indicated that the solution is rather insensitive to this parameter. Additional discussion of parameter selection will be given later on when we present the solutions. Attention will now be directed to the method of solution.

Consideration was first given to the momentum equations (19) and (21). A dimensionless film thickness η_δ was selected. Then a guess was made for the dimensionless suction velocity $f(0)$, and a guess was made for the dimensionless shear stress at the metal surface $f''(0)$. These values, together with the condition $f'(0) = 0$, provide three initial conditions for the gas–vapor film momentum equation (21). With these conditions, equation (21) was integrated in the positive η-direction to the location of the vapor–liquid interface $\eta = \eta_\delta$. The values of f, f', and f'' at this location can be transformed by matching conditions (25) into values of $F(0), F'(0)$, and $F''(0)$ once the ratios ε and β are assigned. The liquid momentum equation (19) was integrated with respect to ξ. It was then necessary to check whether $F'(\xi)$ approaches the asymptote $F' = 1.0$ at large ξ. If not, a new guess was made for the dimensionless shear stress at the metal surface $f''(0)$, holding both η_δ and $f(0)$ constant, and the entire integration was repeated until the condition $F'(\infty) = 1.0$ was fulfilled. Once the correct value for $f''(0)$ was found, the solutions $f(\eta)$ and $F(\xi)$ were used as input data for the solution of the energy and diffusion equations (20), (22), and (23). The values of Y_i [from equation (27)] and $\omega'(0)$ obtained from this solution were then substituted into equation (24) to see if we recovered the assumed value of the suction velocity $f(0)$. If not, a new value of $f(0)$ was chosen and the calculations were repeated until all the matching conditions and boundary conditions were satisfied for the prescribed value of η_δ. The reliability of the numerical forward integration scheme was established by reproducing the closed-form results of Epstein and Hauser [11] for the limiting case of film boiling in the stagnation region of a non-reactive surface.

For an assigned value of the dimensionless vapor–gas film thickness η_δ, the solutions of the differential equations provide the quantities Y_i, $\theta'(0)$, $\theta'(\eta_\delta)$, $f(\eta_\delta)$, $\phi'(0)$, $\omega'(0)$, and $\omega'(\eta_\delta)$. Thus, it is clear that these output quantities obtained from the solutions are unique functions of η_δ. The final equations which remain to be used are equation (7), which relates T_i to Y_i at the vapor–liquid interface, and the energy matching condition (28). These relations, coupled with the solutions described in the foregoing, are sufficient for the determination of the interface temperature T_i.

Consider the problem involving a specific hot reactive surface and flowing liquid system wherein the following quantities are specified: P_∞, T_∞ and T_w. The actual computational procedure by which this problem was solved was as follows: a table of $\theta'(\eta_\delta), f(\eta_\delta)$ Y_i and $\phi'(0)$ as a function of η_δ was constructed from the numerical integrations. Then, for any chosen value of η_δ, the corresponding values of these quantities were easily determined from the table by interpolation. From the matching condition (28), it follows that T_i is a unique function of η_δ. Equation (7) provides another relation between T_i and η_δ. The two equations were solved for η_δ and T_i. The table values were 'stored' in a computer and the entire procedure was carried out on the computer.

Quasi-steady theory of reacting metal spheres in water

In this section the foregoing steady-state analysis is extended and combined with the Baker–Just [6]

parabolic rate law and applied to the prediction of the oxidation rate of hot Zr metal spheres (droplets) falling through water. The theoretical description of an isolated Zr sphere surrounded by a film of steam and hydrogen is based on the model introduced by Epstein and Hauser [11] for forced convection film boiling from a sphere. They approached the film boiling problem from the point of view that the vapor film thickness is a weak function of the arc length measured from the front stagnation point up to the equatorial plane of the sphere, where the vapor film is transformed into a thick vapor wake (separation point). Thus it is assumed that most of the heat and mass is transferred on the lower half of the falling spheres at rates determined from the solution of the governing equations for stagnation flow.

Although the downstream side of spheres during forced convection film boiling have been observed to be covered by thick vapor wakes [10, 12] photomicrographs of the reacted Zr particles [5, 6] do not indicate any variation of the thickness of the oxide layers around the particle surface. Perhaps the falling spheres were somehow set into rotational motion (spinning). Spherical symmetry, therefore, is the simplifying assumption that will be adopted in the following treatment of the growth of the oxide film beneath the sphere surface.

It should be mentioned that the majority of the molten Zr drops produced in the experiments of Baker and Just [6] were of sizes 1 mm or less. To the best of the authors' knowledge, there is no information in the literature concerning the formation of wakes occupying the downstream side of such small spheres. However, since wake formation is a direct consequence of the flow reversal that must take place just past the equator of large or small spheres, it is assumed to occur on the downstream side of the small spheres (drops) of interest here. We also note that the results of the calculations show that the vapor–product gas film thickness can be an appreciable fraction of the reacting sphere radius, in contradiction to the stagnation flow model which does not account for sphere curvature effects. Nevertheless, it is felt that the insights gained from the model regarding film boiling on a reactive surface, together with the asymptotic applicability of the present formulation to large droplets (of any shape), amply justify our preliminary study of the planar surface case.

During its fall, the sphere gains energy from the exothermic oxidation reaction equation (1) and loses energy by means of radiation and convection. Since the surface temperature of the sphere is continually changing with time, thermal convection in the liquid and heat and mass transport in the film should be unsteady. Moreover, the Baker–Just experiments [6] were performed in small volume, sealed vessels partly filled with liquid water but with no inert gases present. As hydrogen was generated by the reaction, the system pressure P_∞ increased. Notwithstanding the variation of T_w and, perhaps, P_∞ with time, it is reasonable to suppose that a quasi-steady state is attained in which the steady-state conservation equations (19)–(23) determine the instantaneous mass and heat per second entering and leaving the sphere, respectively. In fact, it can be shown that the time necessary for a diffusion wave to span the film dimension δ or the liquid boundary layer thickness is much smaller than the sphere oxidation (or heating) time, so that there is little doubt of the validity of this assumption.

In the model reported in the previous sections, the vapor mass fraction Y was set equal to zero at the reacting surface as a result of the assumption that gas phase diffusion within the film controls the reaction rate. This constraint on the vapor mass fraction must be removed in the transition regime between 'chemical control' and diffusion control (mixed control) and when the surface reaction exerts complete control. The boundary layer theory will now be generalized to include a nonzero reactant vapor concentration at the reactive surface.

In order to determine the concentration of the reactant vapor at the reactive surface, Y_w, we write Fick's law (5) at this location:

$$\dot{m}_v - Y_w(\dot{m}_v + \dot{m}_g) = -\rho D\left(\frac{\partial Y}{\partial z}\right)_{z=0}. \tag{32}$$

We now define a new dimensionless vapor mass fraction

$$\omega = \frac{Y - Y_w}{Y_i - Y_w}. \tag{33}$$

Recall that our previous definition was $\omega = Y/Y_i$, i.e. Y_w was assumed to be zero. Note that ω still obeys equation (23) and is still subject to the boundary conditions $\omega(0) = 0$ and $\omega(\eta_\delta) = 1.0$ expressed by the last of equations (24) and (26). Substituting equation (33) into (32), introducing definition (16) for η, eliminating $\dot{m}_v$ and $\dot{m}_g$ in favor of $f(0)$ through equation (10) and the last of (16), and, finally, solving the result for Y_w yields

$$Y_w = \frac{Sc\, f(0)/(1 - M_g/M_v) - \omega'(0) Y_i}{Sc\, f(0) - \omega'(0)}. \tag{34}$$

The above expression relates the reactant vapor mass fraction at the reactive surface to that at the vapor–liquid interface, Y_i, and to the suction velocity $f(0)$ and the reactant vapor concentration gradient $\omega'(0)$ at the reactive surface. Note that equation (34) reduces to the first of boundary conditions (24) when gas phase diffusion controls and therefore $Y_w = 0$; it replaces condition (24) during mixed control. In order to complete the statement of the problem when diffusion does not by itself limit the forward rate of reaction ($Y_w \neq 0$), a phenomenological chemical rate law must be provided.

For many metal oxidation reactions of practical interest the rate of metal reactant consumption is found to depend inversely on the instantaneous thickness of a growing oxide layer beneath the metal surface. This so-called parabolic rate of oxidation has been related to the fact that oxygen has to migrate from the outer oxide

surface to the oxide/metal interface before chemical combination can occur. Hence an oxygen diffusion gradient is set up simultaneously with the growth of oxide. If x is the instantaneous radial location of the oxide/metal interface (oxidation front) measured from the center of a reacting metal sphere, the rate at which metal is replaced by oxide is simply $-4\pi x^2 \rho_m \, dx/d\tau$ (g s^{-1}). From stoichiometry, the vapor mass flux at the surface of the sphere can be expressed in terms of $dx/d\tau$ as [see equation (1)]

$$\dot{m}_v(0) = -n\rho_m \frac{M_v}{M_m} \frac{x^2}{R} \frac{dx}{d\tau}, \tag{35}$$

where the negative sign is included so as to yield a positive quantity for the inward vapor mass flux. The rate law $dx/d\tau\ (x, T_m)$ for the zirconium–water system has been determined by Baker and Just [6] to be approximately parabolic, with an Arrhenius relation temperature dependence, and well-represented by

$$-(R-x)\frac{dx}{d\tau} = C \exp\left(-\frac{\Delta E}{\bar{R}T_m}\right). \tag{36}$$

Here $C = 3.94 \times 10^{-4}$ m^2 s^{-1}, the activation energy $\Delta E = 190\,400$ kJ kg^{-1} mol^{-1}, R is the radius of the reacting zirconium sphere, and $\bar{R}$ is the universal gas constant. Strictly speaking, equation (36) represents the parabolic rate law for plane geometry. The error introduced by applying this simplifed law to a sphere is less than 25% until half of the sphere is oxidized [6], and therefore the effect of spherical geometry is ignored.

Under isothermal conditions, $dx/d\tau$ in equation (36) is a decreasing function of time, reflecting the protective role of the adherent oxide film that grows beneath the surface. Also, we note that equation (36) is a zero-order reaction law in that $dx/d\tau$ is independent of the water–vapor concentration Y_w at the reactive surface. Thus we anticipate a sudden exchange of control between diffusion and chemical (internal diffusion) at the location in time where the gas-phase diffusion-limited reaction rate and the parabolic law-limited rate are identical. The process does not enter a transition region between diffusion and chemical control.

It is useful to derive an expression for the suction velocity $f(0)$ in terms of the growth rate of the oxide layer. Upon noting from equations (9) and (10) that $\dot{m}(0) = (1 - M_g/M_v)\dot{m}_v(0)$ and that $\dot{m}(0) = \rho v(0) = -(2av)^{1/2}\rho f(0)$ by definition, we get after substituting equation (35) for $\dot{m}_v(0)$ and using definition (30) for β

$$f(0) = -\frac{n}{(2a_1\nu_1)^{1/2}\beta} \cdot \left(\frac{\rho_1}{\rho}\right)^{1/2} \cdot \frac{\rho_m M_v}{\rho_1 M_m} \cdot \left(1 - \frac{M_g}{M_v}\right) \cdot \left(\frac{x}{R}\right)^2 \frac{dx}{d\tau}. \tag{37}$$

To complete the statement of the reacting sphere problem, it remains to specify the equations for the determination of the instantaneous sphere temperature T_m. It will be assumed for simplicity that the temperature inside the metal sphere is uniform ($T_m = T_w$) or that a mean sphere temperature can be assigned. Most of the Zr metal spheres under consideration are small enough such that the transient conduction period within the sphere usually occupies less than 10% of the total reaction time. It is clear on physical grounds that the rate of change of sphere enthalpy must be equal to the heat released by exothermic reaction minus the heat convected and radiated through the H_2O–H_2 film, i.e.

$$\tfrac{4}{3}\pi R^3 \rho_m c_m \frac{dT_m}{d\tau} = 2\pi R^2 \cdot \frac{\dot{m}_v \Delta H}{nM_v} - 2\pi R^2 \dot{q} - 4\pi R^2 \dot{q}_{rad}, \tag{38}$$

where the flux terms $2\pi R^2 \dot{m}_v$ and $2\pi R^2 \dot{q}$ follow from the assumption mentioned in the foregoing that convective mass and heat transport are negligible on the downstream side of the reacting metal sphere.* Of course, heat is radiated outward from the entire sphere surface area $4\pi R^2$. A value of 588.0 kJ mol^{-1} of metal reacted is taken as the heat of reaction ΔH [6].

During computation of the chemical heating period and subsequent cooling of the metal sphere, the temperature of the *unreacted* metal may pass through its melting temperature ($T_{mp} = 1857$°C for Zr). When this occurs, it is assumed that heat is absorbed or evolved without a change in metal temperature. Estimation of the time span during which the sphere remains at T_{mp} is made by replacing $c_m \, dT_m/d\tau$ in the first term of equation (38) by $L_m \, dF_m/d\tau$, where L_m is the latent heat of fusion of the metal material and F_m is the fraction of molten metal. This term is used until the unreacted metal is fully melted (during heatup) or fully solidified (during cooldown). Calculated peak temperatures for particles smaller than about 1000 μm in heated water reach about 3500 K, which is about 500 K above the melting point of ZrO_2. However, calculated reaction exceeds 50% of the Zr metal droplet material, so that it makes little difference whether or not the heat of fusion of the oxide material is accounted for since it is very small compared with the energy source due to oxidation.

According to Fourier's law, the outward convective heat flux at the reacting surface is given by $\dot{q} = -k(\partial t/\partial z)_{z=0}$. In terms of the transformed variables of equations (16) and (18) the expression for $\dot{q}$ becomes

$$\dot{q} = \frac{k(T_m - T_i)}{\beta} \cdot \frac{(6Re)^{1/2}}{2R} \cdot f'(0). \tag{39}$$

Similarly, from Fick's law (32) the rate of reactant vapor

* In general, a number that varies with time between $2\pi R^2$ and about $3\pi R^2$ should appear as the multiplier of $\dot{m}_v$ and $\dot{q}$ in equation (38) to account for the fact that the area covered by the wake depends on the degree of subcooling in the liquid [12]. To the level of approximation of the present formulation, this refinement can be ignored.

transport to the surface is

$$\dot{m}_v = \frac{\rho D(Y_i - Y_w)}{1-(1-M_g/M_v)Y_w} \cdot \frac{(6Re)^{1/2}}{2R} \cdot \frac{\omega'(0)}{\beta}, \quad (40)$$

where in the regime of diffusion control $Y_w = 0$.

The numerical procedure used to solve for the sphere temperature and reaction time histories $T_m(\tau)$ and $x(\tau)$, given the initial values $T_m(0)$ and $x(0) = R$, follows. At each time step it is necessary to integrate the two simultaneous first order ordinary differential equations (36) and (38). Suppose that at any time step the state variables of the sphere, T_m and x, are known. Of course, the boundary conditions in the liquid far from the sphere, $T_\infty V_\infty$ and P_∞, are given. The state variable $T_m = T_w$ is regarded as just another boundary condition for the steady-state boundary layer analysis, and equations (19)–(23) are solved to yield the fluxes $\theta'(0)$, $\omega'(0)$; the vapor concentration and temperature at the liquid interface, Y_i, T_i; and the vapor mass fraction at the reactive surface, Y_w. Then $\dot{q}$ and $\dot{m}_v$ are evaluated from equations (39) and (40), and equations (36) and (38) can be integrated through the next time step.

The procedure for obtaining $\theta'(0)$, $\omega'(0)$, etc. when the reaction rate is controlled by counter diffusion in the H_2O–H_2 film ($Y_w = 0$) has already been outlined. A similar procedure can be employed during the period of chemical control. Many integrations of the conservation equations (19)–(23) were carried out for prescribed values of the dimensionless film thickness η_δ and suction velocity $f(0)$, and tables of the quantities $\theta'(\eta_\delta)$, $f(\eta_\delta)$, $\phi'(0)$, $\theta'(0)$, Y_i and Y_w as functions of η_δ and $f(0)$ were constructed. Then, for any given values of η_δ and $f(0)$, the corresponding values of the quantities $\theta'(\eta_\delta)$, $f(\eta_\delta)$, etc. are easily determined from the tables by interpolation. In the regime of chemical control the surface of reacting sphere temperature T_w (or T_m) and the suction velocity $f(0)$ are determined at any time step from equation (38) and equations (36) and (37), respectively. These values together with the tables and the simultaneous solution of equations (7) and (28) yield the quantities Y_i, T_i, Y_w, $\theta'(0)$ and $\omega'(0)$, which are needed to integrate equations (36) and (38) an additional time step.

Both the gas-phase diffusion-limited reaction rate and the parabolic law-limited rate are computed at each time step during the simultaneous integration of equations (36) and (38). Whichever predicted rate is lower, diffusion or chemical, determines the mode of control for the subsequent time step.

It should be noted that although our steady-state boundary layer analysis and the corresponding tables for $\omega'(0)$, $\theta'(0)$, etc. as functions of η_δ and $f(0)$ are based on constant values of the dimensionless groups Pr, Pr_l, Sc, β and ε, the physical properties of the product gas–vapor film and the liquid boundary layer that appear in matching condition (28) and in equations (39) and (40) for the energy and mass fluxes were corrected at each time step. As reference temperatures and concentration for properties evaluation, $0.5(T_w + T_i)$, $0.5(T_i + T_\infty)$ and $0.5(Y_w + Y_i)$ were used, where the required value of Y_w when chemical control prevails was readily obtained from equation (34).

As mentioned previously, in the Baker–Just [6] Zr sphere quenching experiments the ambient pressure P_∞ increased with time due to the accumulation of hydrogen gas within the closed reaction vessel. The calculation of the buildup of hydrogen gas was accomplished by combining equations (9) and (40) to obtain the expression for the instantaneous outward H_2 mass flux, which was integrated simultaneously with equations (36) and (38) for the total hydrogen accumulated at any time per surface area of metal reacted. The metal surface area for hydrogen production was estimated from the reported mean particle diameter and volumes of the original specimen wires [6]. The vessel pressure time history was then determined from the ideal gas law, assuming that the evolving hydrogen was rapidly cooled to the bulk water temperature. During the quasi-steady reacting metal sphere calculation, the interface temperature T_i responds to an increasing P_∞ in accord with equation (7).

RESULTS

Representative velocity, vapor concentration, and temperature profiles for the steady-state stagnation flow of water over a hot Zr surface are to be presented first. The oxidation predictions of the quasi-steady theory of the reaction of molten metal spheres falling through water will then be compared with experiment.

Structure of boundary layer in the stagnation region of an isothermal, reactive sphere

The solutions of equations (19)–(23) provide reactant vapor concentration, temperature and velocity profiles for the vapor–product gas (H_2O–H_2) film and the liquid boundary layer. These solutions can be applied to forced convection film boiling over most of the front surface of a reactive sphere by evaluating the stagnation point velocity gradient a_1 using equation (14). Figures 2–6 display the stagnation region profiles for a 1.0 mm diameter, isothermal Zr sphere in water flowing at $V_\infty = 0.27$ m s^{-1} and $P_\infty = 1$ atm, for the case where the reaction rate is diffusion controlled ($Y_w = 0$). The first two figures are for the velocity profiles and the last three are for the temperature and reactant vapor concentration profiles. All figures are for a vapor–gas film Schmidt number of 0.4 and Prandtl number of 0.7. Inasmuch as the thickness of the H_2O–H_2 film and its velocity and temperature levels are one order of magnitude more than the thickness of the liquid boundary layer and its velocity and temperature levels, separate ordinate and abscissa scales had to be employed for each region.

Figure 2 shows profiles of the velocity corresponding to a constant metal temperature $T_w = 1925$°C and saturated water $T_\infty = 100$°C. We note that the thickness of the vapor–gas film in this case is $\delta \simeq 0.1$ mm. In stagnation flow the tangential velocities u

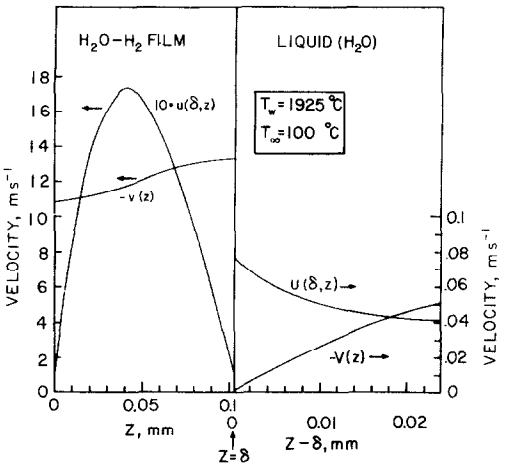

FIG. 2. Representative velocity profiles in the neighborhood of the forward stagnation point of a sphere: $V_\infty = 0.27$ m s^{-1}, $P_\infty = 1$ atm.

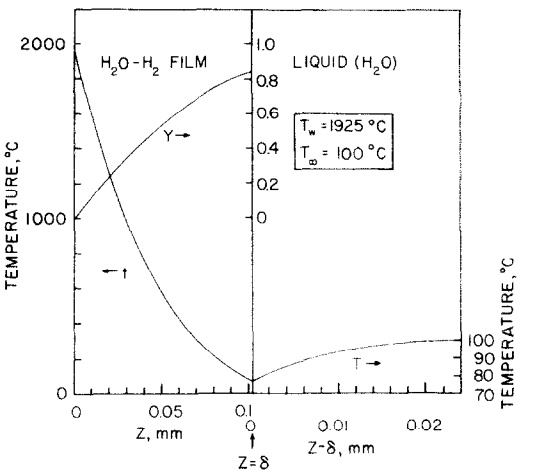

FIG. 4. Representative temperature and vapor concentration profiles in the neighborhood of the forward stagnation point of a sphere, saturated bulk liquid: $V_\infty = 0.27$ m s^{-1}, $P_\infty = 1$ atm.

and U increase linearly with r from zero at $r = 0$ [see equations (15) and (16)]. The tangential velocity profile at a radial distance from the origin equal to the thickness of the film is shown in Fig. 2. Due to the free stream pressure distribution impressed on the film and the low density of the film compared to that of the liquid, the tangential film velocity exhibits a maximum and greatly exceeds the liquid tangential velocity. The normal velocity profile within the film differs from that of conventional film boiling in that the velocity is not zero at the hot surface. The flatness of the normal velocity profile within the film is an index of the importance of chemical suction relative to that of liquid evaporation. For higher metal temperatures, the film thickness must increase in order to accommodate increased vapor production rates (see Fig. 3).

The temperature and reactant vapor concentration profiles corresponding to the velocity profiles of Fig. 2 are shown in Fig. 4. It may be seen that the temperature and concentration profiles in the film are not straight, indicating that convection, suction and blowing play a large role in the transport of heat and mass. As the metal temperature increases, the evaporating liquid surface receives less and less heat (compare Fig. 4 with Fig. 5). The metal surface gives up more and more heat which is swept away in the radial direction in the form of increased enthalpy of the fluid. It is interesting to note that because of the strong suction at the metal surface, in considering the total rate of heat loss from the surface, convection dominates over radiation, even at metal temperatures as high as 3200°C.

Perhaps the most interesting new phenomenon to emerge in considering the effects of the reactive surface in film boiling concerns the temperature profile in the liquid. One normally expects no liquid heat transfer in the case of saturated liquids. This is *not* necessarily the case here since significant concentrations of the product gas, H_2, may build up at the evaporating liquid surface. Corresponding to the buildup of the product gas, the mass fraction of the vapor at the liquid surface must be

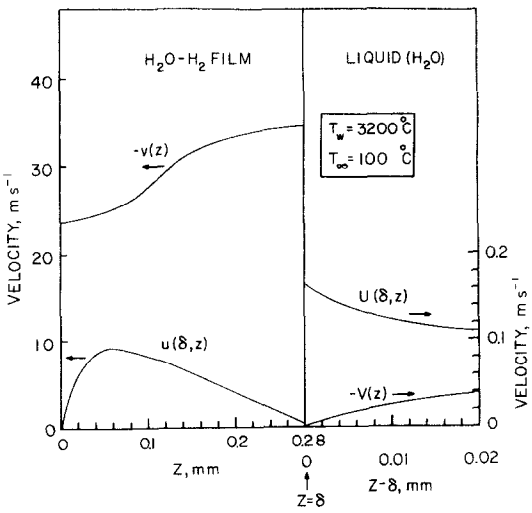

FIG. 3. Representative velocity profiles in the neighborhood of the forward stagnation point of a sphere: $V_\infty = 0.27$ m s^{-1}, $P_\infty = 1$ atm.

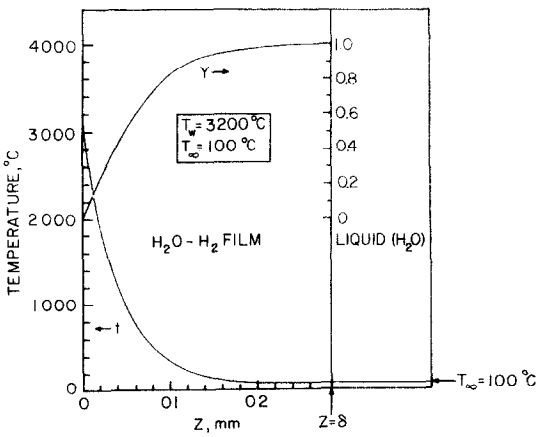

FIG. 5. Representative temperature and vapor concentration profiles in the neighborhood of the forward stagnation point of a sphere with high surface temperature, saturated bulk liquid: $V_\infty = 0.27$ m s^{-1}, $P_\infty = 1$ atm.

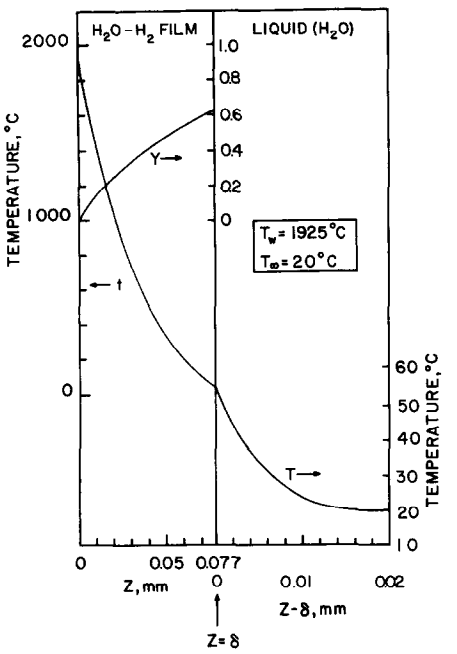

FIG. 6. Representative temperature and vapor concentration profiles in the neighborhood of the forward stagnation point of a sphere, highly subcooled bulk liquid: $V_\infty = 0.27$ m s^{-1}, $P_\infty = 1$ atm.

reduced (see Fig. 4). There will be a consequent reduction of the interface temperature T_i and a corresponding inward flux of heat from the liquid to the evaporating surface since the thermal driving force $(T_i - T_\infty)$ is nonzero and negative. In this interesting situation, the evaporating surface receives heat from both the hot metal and the 'saturated' liquid. This effect is reduced at higher metal temperatures where the inward evaporation (blowing) process is sufficiently high to overcome the diffusive flow of H_2 product toward the vapor–liquid interface. We note from Fig. 5 that at a metal temperature $T_w = 3200$°C the concentration of product gas at the evaporating surface is very small such that $Y_i \simeq 1.0$, and the temperature profile in the liquid is uniform and equal to T_∞.

In Fig. 6 temperature and reactant vapor concentration profiles are plotted for $T_w = 1925$°C and a water subcooling of 80°C ($T_\infty = 20$°C). In this highly subcooled condition some of the energy transferred from the metal heats the flowing liquid. Again, the buildup of noncondensable product gas at the film–liquid interface prevents the interface temperature from rising to the saturation temperature, 100°C, corresponding to the ambient pressure. However, the mass fraction of vapor at the film–liquid interface achieves a level sufficient to support significant oxidation of the metal; it is about 4.0 times larger than that predicted by assuming the water surface remains at the bulk water temperature $T_\infty = 20$°C.

Oxidation history of a nonisothermal reaction sphere—comparisons with experiment

Here we present the predictions of the steady-state boundary layer equations for the film and liquid regions together with the unsteady energy balance (38) on the reacting sphere.

Calculated temperature–time and percent reaction–time histories for Zr spheres of different diameters are plotted in Fig. 7. The calculations were carried out for the experimental conditions reported by Baker and Just [6]. As mentioned previously, 2.54 cm lengths of either 30 or 60 mil Zr wires were rapidly heated and melted under water. The experiments were conducted in sealed test cells partly filled with liquid water and degassed so that the water was initially saturated. Early in the reaction transient, the predicted temperature profile within the liquid boundary layer surrounding a falling molten Zr sphere generated by the rapid heating is such that heat is convected from the liquid to the gas–vapor film, as shown in Fig. 4. As the pressure in the cell increases due to hydrogen production, the liquid subcooling increases from zero and the liquid temperature profile gradually flattens and for a brief instant, becomes uniform. With further increases in cell pressure and liquid subcooling, the temperature gradient changes sign and heat is predicted to 'flow' from the film into the liquid, as in the highly subcooled situation shown in Fig. 6.

Since the parabolic law reaction rate is infinite at time zero, the initial reaction is predicted to be controlled by gas-phase diffusion in the film enveloping the falling Zr sphere. Initially, the spheres are assumed to be fully melted at their melting temperature. The transient energy balance equation reveals that heat is generated within the spheres by oxidation at a greater rate than it is lost by convection and radiation. Each curve in Fig. 7

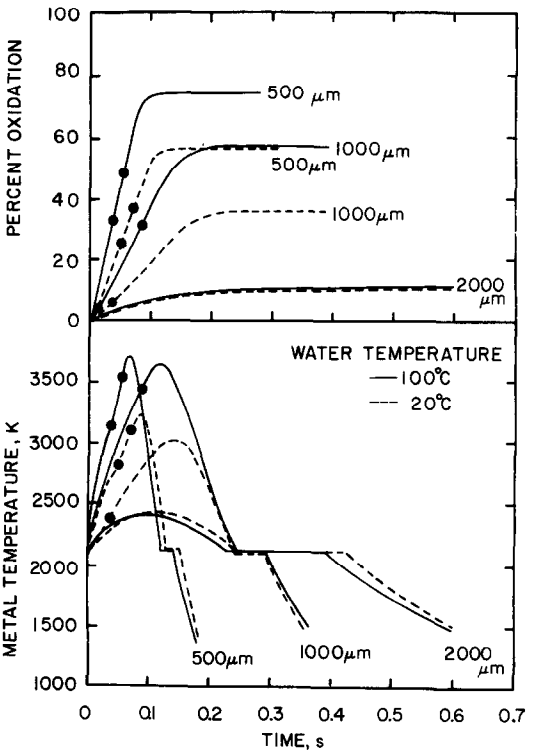

FIG. 7. Effect of sphere size and water temperature on sphere oxidation and temperature time histories.

is marked to show when the exchange of control from external diffusion to internal oxidation kinetics first occurs. This is followed by a period in time (between the circle marks on the curves in Fig. 7) in which the diffusion-controlled rate and the parabolic law-controlled rate are essentially in balance. When the process first enters the chemical regime, the reaction rate slows down and the net influx of mass to the sphere (suction) diminishes. This is accompanied by a decrease in the energy flux from the sphere, due to a reduction in the local film temperature gradient, an abrupt incremental increase in the rate of rise of the sphere temperature and a return to diffusion control. Thus the time period between the circles in Fig. 7 is characterized by a cyclic solution between diffusion and chemical control. Ultimately, however, the parabolic rate becomes too low for the self-regulating effects of surface suction to drive the process back and forth between diffusion and chemical control. Thereafter, the reaction rate decelerates rapidly, leading to a stage of net sphere cooling and subsequent solidification.

The results in Fig. 7 indicate that the extent of reaction is very sensitive to the sphere diameter. For sizeable Zr spheres, the time necessary to self-heat the sphere by reaction is long compared with the time for the parabolic law reaction speed (evaluated at the initial sphere temperature) to drop below the reaction speed limited by gas-phase diffusion. This early transition to parabolic kinetics limitations greatly reduces the final extent of oxidation in large spheres. In small spheres the temperature rises abruptly and the time to reach the period of chemical control is delayed until a relatively large fraction of the sphere is oxidized.

Measurements of the final extent of reaction of molten Zr spheres suddenly released into water have been reported in refs. [5, 6]. The extent of reaction was found to depend primarily on the water temperature and the sphere diameter. This dependence is represented graphically in Fig. 8. The full lines represent the theoretical results, which show rough agreement with the experimental data. Most of the experimental points lie somewhat below the curves. As remarked earlier, the key dimensionless parameter Sc that appears in the boundary layer equations for the H_2O–H_2 film was assumed constant and equal to 0.4. Parametric studies show that there exists a different choice of Sc, that falls within the range of reasonable values for this parameter, which is able to bring theory and experiment closer together. However, given the constraints of the present theory, a comparison of the experimental values with such a 'refined prediction' would not be productive and, perhaps, would be misleading.

It is clear from Fig. 8 that our present theoretical approach is capable of accounting for all the observed features of available controlled Zr water oxidation experiments. The predicted and experimental percent reaction results show that the effect of increasing the bulk water temperature from 20 to 100°C is to increase the extent of reaction, while there is no apparent difference for bulk water temperatures ranging from 100 to 300°C. The curve labeled 'heated water' in Fig. 8 represents the average of three curves of percent reaction versus sphere diameter, corresponding to predictions for $T_\infty = 100, 200, 300$°C, which differ from the 'average curve' by less than 5%.

It is seen from equations (39) and (40) that the temperature and reaction histories of the sphere

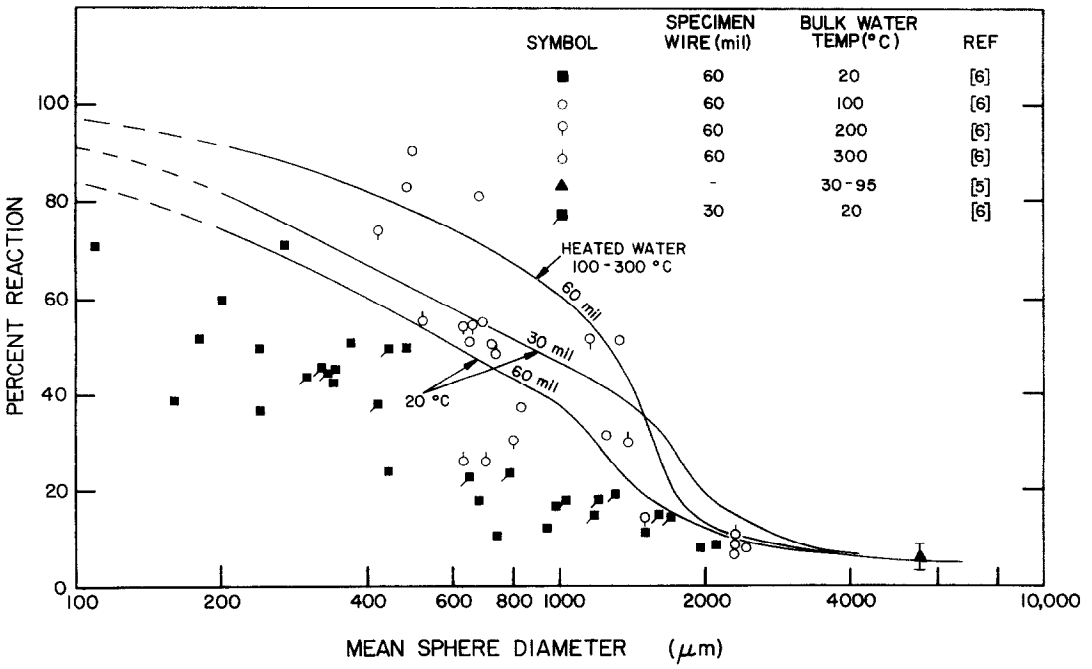

FIG. 8. Final percent reaction vs sphere diameter; comparison of theory with experiment.

depend directly on the values of the quantities k, ρD, β, $\theta'(0)$, $\omega'(0)$, $T_m - T_i$, Y_i, and Re. Inspection of the numerical results shows that, for a fixed specimen wire size, only the last of these quantities, the liquid Reynolds number, is very sensitive to variations in the bulk water temperature, owing to the strong, inverse relationship between liquid viscosity and temperature. As the bulk water temperature T_∞ is increased from 20 to 100°C, the diffusion-controlled rate of reaction tends to increase, due mainly to an increase in Re. The convective heat loss rate from the sphere also increases with increasing T_∞ or, equivalently, with increasing Re. Early in time, however, sphere reaction heating wins out over the convective cooling and the sphere temperature rises faster in heated water than in room temperature water, as can be seen in Fig. 7 by comparing the solid curves with the dashed curves. But later in time, when the heating of the sphere is chemically controlled, the higher convective cooling rate in heated water is in some cases strong enough to cause the temperature–time curve to drop below that of a sphere of the same size falling through room temperature water. Examination of Fig. 7 shows this to be the case for both the 500 and 2000 μm diameter spheres. Since the reaction velocities are higher the higher the temperature of the Zr sphere, early in time, usually before the peaks in the sphere temperature–time curves, more reaction takes place in spheres falling through heated than in spheres falling through room temperature water, while the opposite is true after the sphere temperatures pass through their peak values. In sizeable spheres falling through heated water, the 'extra' oxide accumulated (relative to spheres in room temperature water) before its temperature peaks is just about equal to the 'extra' oxide gained in an identical size sphere released in room temperature water after its temperature peaks, so that there is little difference in the final extent of reaction between the two cases. For the very same reason there is little difference in the calculated final extent of reaction in heated water ranging in temperature from 100 to 300°C over the entire range of sphere diameters investigated. On the other hand, it may be concluded from Fig. 7, simply by comparing the temperature histories of the 500 and 1000 μm size particles in water at 100°C with those in room temperature water, that the extent of reaction is greater in small spheres released in 100°C water. Apparently the observed percent reaction trends relative to water temperature can be related to the fact that heat and mass transfer in the H_2O–H_2 film is strongly affected by the liquid Reynolds number. The enhanced reaction rate in heated water seems to be mainly a *hydrodynamic effect*.

Included in Fig. 8 are two curves representing the calculated results for Zr spheres formed by melting either 30 or 60 mil diameter Zr wires in water at 20°C. The results indicate that somewhat more reaction occurs within molten spheres formed from the 30 mil Zr wires. The experimental data taken from ref. [6] and shown in Fig. 8 seem to indicate a similar trend, although the scatter in the data precludes a definitive judgement concerning the effect of wire diameter on the extent of reaction. The predicted increase in the extent of reaction with decreasing wire diameter may not seem unreasonable when the various factors effecting the reaction rate are discussed. First of all, the 60 mil specimen wires yield a total hydrogen pressure within the reaction cell that is several times larger than the pressure generated by reacting the 30 mil wires. At the higher pressures there is more efficient heat and mass transfer in the H_2–H_2O film owing to an increase in film density ρ. This tends to faster reaction rates in Zr spheres produced from the 60 mil wires, but an overriding effect is in the increase in the convective cooling rate of the spheres which ultimately reduces the extent of reaction below that calculated for Zr spheres generated by heating 30 mil wires.

SUMMARY

The two-phase reactive flow problem which arises in the oxidation of high temperature surfaces immersed in water in film boiling was formulated in terms of steady-state stagnation flow theory. In nearly saturated liquids, the effect of counter-diffusion of product gas and evaporated liquid within the film is to reverse the normal direction of heat transfer so that heat from the liquid is convected *toward* the surface. Available zirconium (Zr) particle oxidation data were shown to be consistent with the theory and a reaction sequence first proposed by Baker and Just [6] in which the oxidation rate is initially limited by the counter-diffusion of water vapor and hydrogen in the film that surrounds the Zr sphere, and later becomes limited by the kinetics of oxide layer buildup on the Zr surface.

REFERENCES

1. W. E. Stewart and R. Prober, Heat transfer and diffusion in wedge flows with rapid mass transfer, *Int. J. Heat Mass Transfer* **5**, 1149–1163 (1962).
2. H. M. Higgins, A study of the reaction of metals and water, Report AECD-3664, Hanford Atomic Products Operation, Richland, Washington, April (1955).
3. W. Milich and E. C. King, Molten metal–water reactions, Report NP-5813, DTI Extension, November (1955).
4. W. C. Ruebsamen, F. J. Shon and J. B. Chrisney, Chemical reaction between water and rapidly heated metals, Report NAA-SR-197, North American Aviation, Los Angeles, California, October (1952).
5. R. C. Crooks, P. G. Hershall, H. A. Sorgenti, A. W. Lemmon, Jr. and R. B. Filbert, Jr. Studies relating to the reaction between zirconium and water at high temperatures (edited by A. W. Lemmon, Jr.), Report BMI-1154, Battelle Memorial Institute, Columbus, Ohio, May (1962).
6. L. Baker, Jr. and L. C. Just, Studies of metal–water reactions at high temperatures III—experimental and theoretical studies of the zirconium–water reaction, Report ANL-6548, Argonne National Laboratory, Argonne, Illinois, May (1962).
7. B. Lustman, Zirconium–water reactions, Report WAPD-137, Bettis Atomic Power Laboratory, Pittsburgh, Pennsylvania, December (1955).

8. W. A. Bostrom, The high temperature oxidation of zircaloy in water, Report WAPD-104, Bettis Atomic Power Laboratory, Pittsburgh, Pennsylvania, March (1954).
9. W. S. Hogan, R. F. Redmond, J. W. Chastain and S. L. Fawcett, Studies relating to the reaction between zirconium and water at high temperatures (edited by A. W. Lemmon, Jr.), Report BMI-1154, Battelle Memorial Institute, Columbus, Ohio, May (1962).
10. L. A. Bromley, N. R. LeRoy and J. A. Roberts, Heat transfer in forced convection film boiling, *Ind. Engng Chem.* **45**, 2639–2646 (1953).
11. M. Epstein and G. M. Hauser, Subcooled forced-convection film boiling in the forward stagnation region of a sphere or cylinder, *Int. J. Heat Mass Transfer* **23**, 179–189 (1980).
12. L. C. Witte, J. C. Hesson, M. B. Silverman and R. O. Ivins, Thermal reactor safety studies, in *Chemical Engineering Division Semiannual Report*, ANL-7425, p. 152. Argonne National Laboratory, Argonne, Illinois (1968).

EBULLITION EN FILM SUR UNE SURFACE REACTIVE

Résumé—Pour aider la compréhension de l'oxydation rapide de matériaux à haute température immergés dans l'eau, on étudie l'écoulement d'un liquide sur un corps réactif; la température du corps est telle que le liquide atteint l'ébullition en film sur la surface. Dans le film qui enveloppe la surface, le liquide évaporé diffuse vers la surface et il y réagit pour former des produits gazeux qui diffusent. Le problème d'écoulement diphasique et de transfert de chaleur et de masse est formulé dans le cadre de la théorie de l'écoulement d'arrêt permanent. La théorie est appliquée à l'oxydation de sphères de zirconium fondu qui tombent dans l'eau et les résultats sont compatibles avec les données expérimentales d'oxydation de sphères de zirconium.

FILMSIEDEN AN EINER REAKTIONSFREUDIGEN OBERFLÄCHE

Zusammenfassung—Zum besseren Verständnis der schnellen Oxidation von in Wasser eingetauchten Hochtemperaturmaterialien wird hier die Strömung einer Flüssigkeit um einen reaktionsfreudigen Körper behandelt; die Temperatur des Körpers wird so gewählt, daß an dessen Oberfläche Filmsieden einsetzt. Der die Oberfläche umschließende Film enthält Flüssigkeitsdampf, der zur Oberfläche diffundiert und dort zu Produktgasen reagiert, die von der Oberfläche wegdiffundieren. Das auftretende Problem der Zweiphasenströmung und des Wärme- und Stofftransports wird im Rahmen der stationären Theorie für ruhende Strömung behandelt. Die Theorie wird auf die quasistationäre Oxidation von in Wasser fallenden, geschmolzenen Zirkonkugeln angewandt. Die erhaltenen Ergebnisse stimmen mit vorhandenen Daten für die Oxidation von Zirkonkugeln überein.

ПЛЕНОЧНОЕ КИПЕНИЕ НА ХИМИЧЕСКИ АКТИВНОЙ ПОВЕРХНОСТИ

Аннотация—Для лучшего понимания процесса быстрого окисления сильно нагретых погружаемых в воду материалов проведено исследование обтекания жидкостью реакционноспособного тела, нагретого до такой температуры, что на его поверхности происходит пленочное кипение жидкости. В окружающей поверхность тела пленке находится испаряющаяся жидкость, которая диффундирует к поверхности и вступает с ней в реакцию, в результате которой образуется газ, который диффундирует в обратном от поверхности направлении. Задача двухфазного течения и тепло-и массопереноса формулируется в рамках теории стационарного течения с торможением. По используемым соотношениям рассчитывается квазистационарный процесс окисления нагретых до температуры плавления циркониевых шариков, сбрасываемых в воду. Результаты согласуются с имеющимися экспериментальными данными по окислению циркониевых шариков.